

Article

Performance of Siloxane Mixtures in a High-Temperature Organic Rankine Cycle Considering the Heat Transfer Characteristics during Evaporation

Theresa Weith *, Florian Heberle, Markus Preißinger and Dieter Brüggemann

Lehrstuhl für Technische Thermodynamik und Transportprozesse, Zentrum für Energietechnik, Universität Bayreuth, Universitätsstraße 30, 95447 Bayreuth, Germany;

E-Mails: florian.heberle@uni-bayreuth.de (F.H.); markus.preissinger@uni-bayreuth.de (M.P.); brueggemann@uni-bayreuth.de (D.B.)

* Author to whom correspondence should be addressed;

E-Mail: theresa.weith@uni-bayreuth.de or lttt@uni-bayreuth.de;

Tel.: +49-921-55-7161; Fax: +49-921-55-7165.

Received: 30 June 2014; in revised form: 5 August 2014 / Accepted: 18 August 2014 /

Published: 26 August 2014

Abstract: The application of the Organic Rankine Cycle to high temperature heat sources is investigated on the case study of waste heat recovery from a selected biogas plant. Two different modes of operation are distinguished: pure electric power and combined heat and power generation. The siloxanes hexamethyldisiloxane (MM) and octamethyltrisiloxane (MDM) are chosen as working fluids. Moreover, the effect of using mixtures of these components is analysed. Regarding pure electricity generation, process simulations using the simulation tool Aspen Plus show an increase in second law efficiency of 1.3% in case of 97/03 wt % MM/MDM-mixture, whereas for the combined heat and power mode a 60/40 wt % MM/MDM-mixture yields the highest efficiency with an increase of nearly 3% compared to most efficient pure fluid. Next to thermodynamic analysis, measurements of heat transfer coefficients of these siloxanes as well as their mixtures are conducted and Kandlikar's correlation is chosen to describe the results. Based on that, heat exchanger areas for preheater and evaporator are calculated in order to check whether the poorer heat transfer characteristics of mixtures devalue their efficiency benefit due to increased heat transfer areas. Results show higher heat transfer areas of 0.9% and 14%, respectively, compared to MM.

Keywords: Organic Rankine Cycle; siloxanes; high temperature heat source; zeotropic mixtures; heat transfer coefficients; heat exchange area

1. Introduction

The use of zeotropic mixtures in Organic Rankine Cycle (ORC) applications has been widely investigated during the last years. The focus of this research is mainly on low temperature applications like geothermal systems [1–4]. In these cases an efficiency increase of up to 20% is possible by using mixtures compared to the most efficient pure component due to a better glide matching during condensation and evaporation caused by non-isothermal phase change of zeotropic mixtures. Recent investigations also figure the combination of zeotropic mixtures and a transcritical mode of operation due to a better matching of temperature profiles [5,6]. Next to the non-isothermal phase change during condensation resulting from the use of zeotropic mixtures, the evaporation phase change also occurs non-isothermally, due to the supercritical mode of operation. This results in an increase in second law efficiency of up to 60% [5]. Beside geothermal power generation, the benefit of using zeotropic mixtures is also investigated for other specific applications, like for example in the field of heat recovery from engines [7,8]. Furthermore, the first studies that focus on zeotropic mixtures for high temperature ORC have been published. Along with Angelino and Colonna [9,10], who investigated multi-component mixtures of linear siloxanes, Dong *et al.* [11] show results of the performance of hexamethyldisiloxane (MM)/octamethyltrisiloxane (MDM)-mixtures at a heat source temperature of 280 °C. Compared to low temperature applications, the efficiency increase achieved with mixtures in high temperature ORCs is less. Chys *et al.* [12] describe a benefit of nearly 16% for a heat source temperature of 150 °C, whereas at 250 °C the increase is less than 6%.

Next to this advantage of zeotropic mixtures with respect to cycle efficiency, there is also an inherent drawback of using them in ORC-applications caused by their generally reduced heat transfer characteristics compared to pure fluids [13,14]. This fact is often neglected when analysing mixtures in ORC-systems, but regarding sizing of heat exchangers the knowledge of this degradation in heat transfer coefficient is important. Looking at common refrigerants, measurements of heat transfer coefficients of those as well as their mixtures are already available in literature as their long-serving use in refrigeration-systems has driven this research [15–20]. However, in case of siloxane mixtures as well as pure siloxanes up to now there has been a lack of data.

The present study shows a thermodynamic analysis of a high temperature ORC using the linear siloxanes hexamethyldisiloxane (MM) and octamethyltrisiloxane (MDM) as well as their mixtures. Moreover, the results of measurements of heat transfer coefficients of these fluids and their mixtures in steps of 20 wt % MM are presented. Kandlikar's correlation is adapted to the experimental values and is then used for calculating the required heat exchanger area for preheating and evaporation.

2. Thermodynamic Process Analysis

In this study the recovery of waste heat from biogas plants is chosen exemplarily as one application of the ORC. The specifications of the exhaust gas from the biogas-engine (MAN E 2842 LE 322, MAN Truck & Bus AG, Nuremberg, Germany) of the selected biogas plant are summarized in Table 1.

Table 1. Parameters of heat source (EG).

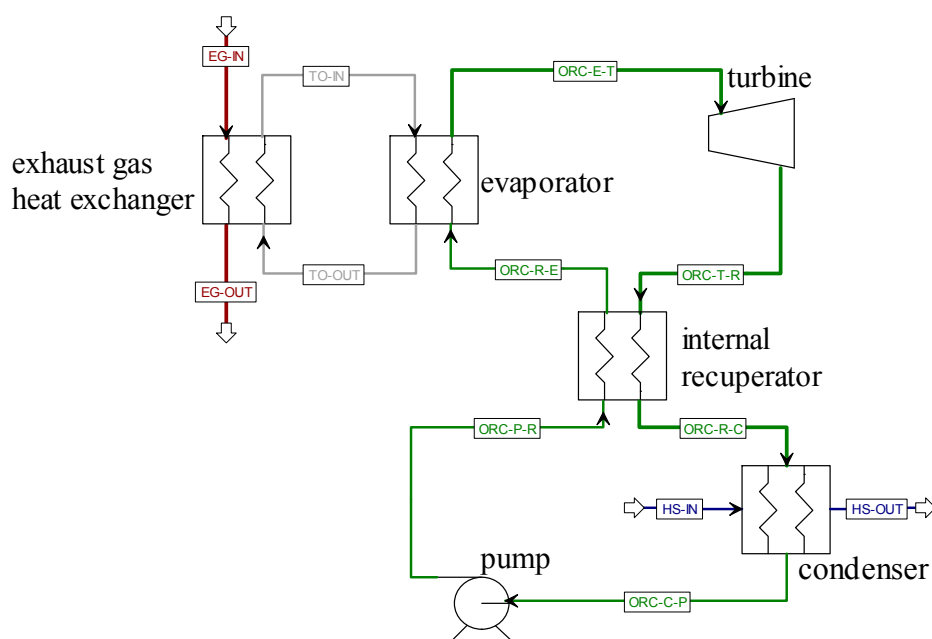
T_{EG-IN} (K)	\dot{m}_{EG} (kg/s)	p_{EG} (bar)	Composition (mol %)				
733.15	0.48	1	N ₂ 64.55	H ₂ O 18.15	CO ₂ 9.74	O ₂ 6.63	Ar 0.93

Siloxanes were chosen as a working fluid due to their good performance in high temperature applications [9,21,22]. In particular, the two linear siloxanes hexamethyldisiloxane (MM) and octamethyltrisiloxane (MDM) as well as their mixtures are investigated. First degradation measurements of MM show its thermal stability up to a temperature of 300 °C [23]. Therefore, with regard to the high heat source temperature, an additional intermediate circuit is considered in the simulations in order to prevent the working fluid from decomposition. Dowtherm G is chosen as thermal oil due to its high thermal stability [24].

2.1. Methodology

Simulations have been performed using the simulation tool Aspen Plus [25]. As property method the PENG-ROB (Peng-Robinson equation of state) model is used for the exhaust gas, air, and Dowtherm G as well as the ORC-fluid. In the case of water, STEAM-NBS (NBS/NRC Steam Tables) is applied [26]. Figure 1 shows the flowsheet of the process. It consists of the ORC, in which an internal recuperator is applied for the purpose of efficiency improvement, and the additional thermal oil loop. All heat exchangers are operating in counter flow mode and pressure drops are neglected.

Figure 1. Aspen Plus flowsheet.



For the heat sink, two different scenarios are analysed. The first one represents pure electricity generation out of waste heat assuming direct air cooled condensation, whereas the second one considers an additional use of the condenser duty in a heating network using water. Table 2 lists the general parameters of the heat sink for those two cases.

Table 2. Heat sink (HS) parameters.

Case	Fluid	T_{HS-IN} (K)	T_{HS-OUT} (K)	\dot{m}_{HS} (kg/s)	p_{HS} (bar)
heat sink (electricity)	air	288.15	303.15	variable	1
heat sink (CHP)	water	323.15	343.15	variable	2

As boundary conditions, the pinch point differences in the heat exchangers are kept constant (Table 3). Only the pinch point differences in the condenser and internal recuperator can reach values higher than those given in Table 3. In the condenser this occurs due to the limitation of the lower working pressure to a minimum value of 0.1 bar. Regarding fluid mixtures, partial condensation can take place in the internal recuperator. If this occurs, the boundary condition is switched. Instead of the fixed pinch point temperature difference a vapour fraction of one is set for the hot outlet stream of the recuperator (ORC-R-C). As a result, pinch point differences can reach higher values. Due to the heat source parameters, the investigated systems are small-scale ORCs with an electrical power output in the kilowatt range. Therefore, the isentropic efficiency of the turbine is set to the relatively small value of 60%.

Table 3. Boundary conditions.

PP_{EG} heat exchanger (K)	$PP_{evaporator}$ (K)	$PP_{condenser}$ (K) (min)	$PP_{internal}$ recuperator (K) (min)	$\eta_{turbine}$ (%)	$\eta_{generator}$ (%)	η_{pump} (%)	η_{driver} (%)
20	30	10	10	60	90	70	90

To compare the simulation results of the different fluids, the exergetic efficiency is chosen as a criterion. For pure generation of electric energy, the exergetic efficiency is defined by the net power P_{net} (power of turbine $P_{el,turb}$ minus power of pump P_{pump}) divided by the exergy of heat source \dot{E}_{EG} :

$$\eta_{ex,electricity} = \frac{P_{net}}{\dot{E}_{EG}} = \frac{P_{el,turb} - P_{pump}}{\dot{m}_{EG}[h_{EG,in} - h_0 - T_0(s_{EG,in} - s_0)]} \quad (1)$$

For calculating \dot{E}_{EG} , mass flow rate \dot{m}_{EG} , enthalpy $h_{EG,in}$ as well as entropy of heat source $s_{EG,in}$ are used. The index 0 corresponds to the reference state (288.15 K, 1 bar). In the case of combined heat and power generation the exergy content of the condenser duty \dot{E}_{cond} has to be taken into account:

$$\eta_{ex,CHP} = \frac{P_{net} + \dot{E}_{cond}}{\dot{E}_{EG}} \quad (2)$$

$$\dot{E}_{cond} = \dot{m}_{HS}[h_{HS,out} - h_{HS,in} - T_0(s_{HS,out} - s_{HS,in})] \quad (3)$$

It is calculated by using inlet and outlet enthalpies ($h_{HS,in/out}$) and entropies ($s_{HS,in/out}$) of the cooling water as well as its mass flow rate \dot{m}_{HS} .

For evaluating the performance during evaporation and condensation, the irreversibilities of the evaporator and condenser are calculated by using respective inlet and outlet enthalpies and entropies:

$$\dot{i}_{\text{evap}} = T_0 \dot{m}_{\text{ORC}} \left[s_{\text{ORC-E-T}} - s_{\text{ORC-R-E}} - \frac{h_{\text{ORC-E-T}} - h_{\text{ORC-R-E}}}{T_{\text{m,evap}}} \right] \tag{4}$$

$$\dot{i}_{\text{cond}} = T_0 \dot{m}_{\text{ORC}} \left[s_{\text{ORC-C-P}} - s_{\text{ORC-R-C}} - \frac{h_{\text{ORC-C-P}} - h_{\text{ORC-R-C}}}{T_{\text{m,cond}}} \right] \tag{5}$$

The logarithmic mean temperatures are defined as follows:

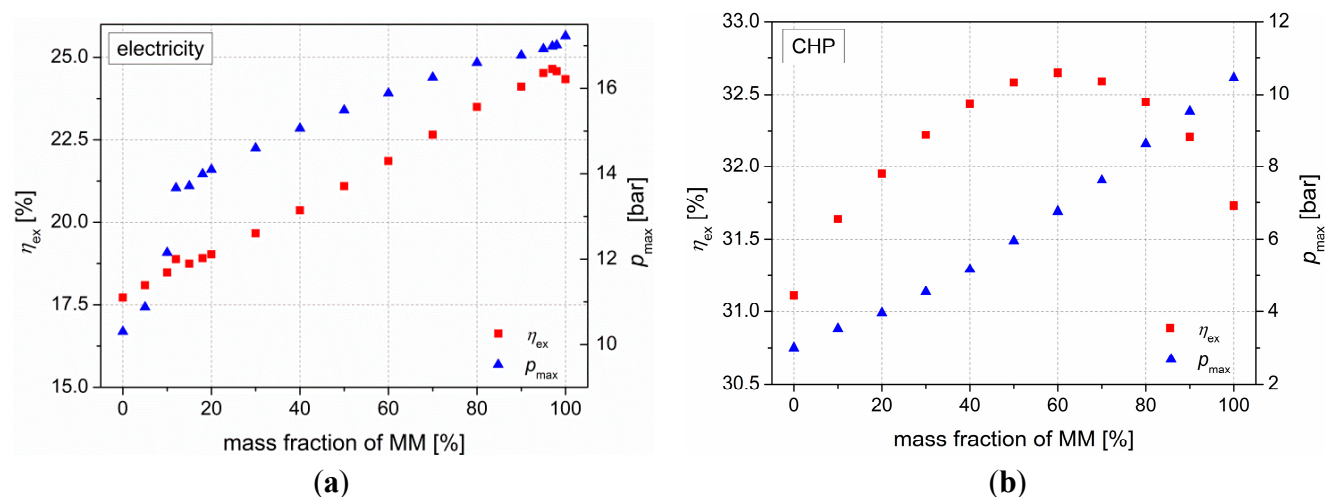
$$T_m = \frac{T_{\text{in}} - T_{\text{out}}}{\ln\left(\frac{T_{\text{in}}}{T_{\text{out}}}\right)} \tag{6}$$

In case of the condenser T_{in} and T_{out} describe the inlet and outlet temperatures of the heat sink. For the irreversibilities of the evaporator the temperatures of Dowtherm G have to be used.

2.2. Results of Process Simulation

Due to the available heat source, the applied ORC shows power outputs in the low power range ($P_{\text{net}} < 30$ kW). The results of the process simulation are displayed in Figure 2. On the left hand side the exergetic efficiency against the mass fraction of MM in case of pure electricity generation is presented, whereas the results for the combined heat and power case are shown on the right hand side. Next to the efficiency, the corresponding upper working pressure, that yields the highest efficiency in each case, is added in the diagrams.

Figure 2. Exergetic efficiencies and respective maximum working pressures against mass fraction of MM ((a): pure electricity generation, (b): combined heat and power generation).

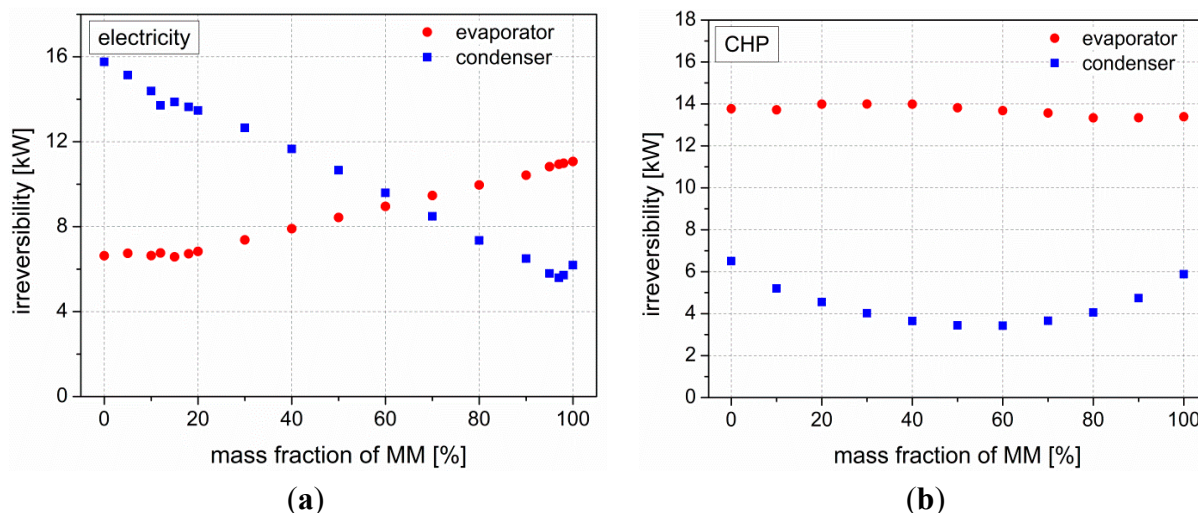


Regarding the case of pure electricity generation and using steps of mass fraction of MM of 10%, it seems that there is a nearly linear behaviour of exergetic efficiency with respect to mass fraction of MM. A closer look reveals that at high mass fractions of MM there might be a deviation from this trend. Therefore, additional steps of 95%, 97% and 98% MM are added and an efficiency increase of nearly 1.3% compared to the most efficient pure component, MM, occurs for 97% MM. A similar effect between mass fractions of 10% and 20% occur, but efficiencies do not exceed that of MM.

A quite different trend with respect to mass fraction of MM can be seen for the combined heat and power production. Compared to the pure fluid with the best exergetic efficiency (MM: $\eta_{\text{ex}} = 31.73\%$)

an efficiency increase of 2.9% is possible when using mixtures (60 wt % MM: $\eta_{\text{ex}} = 32.65\%$). Next to this improved cycle efficiency, lower working pressures are needed compared to pure MM. As shown in Figure 3, this increase in second law efficiency derives from an irreversibility minimum in the condenser. Regarding the irreversibilities in the evaporator, smaller differences between the fluids can be observed. Therefore, they do not affect the overall cycle efficiency.

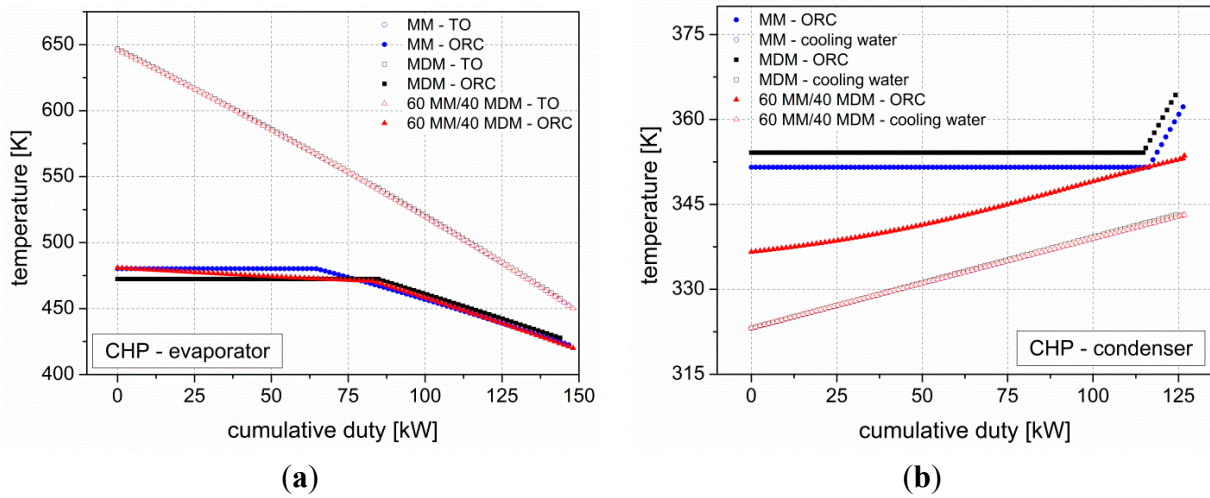
Figure 3. Irreversibilities in evaporator and condenser in case of (a) pure electricity generation and (b) combined heat and power generation.



The reason for this behaviour can be revealed by regarding the temperature profiles during evaporation and condensation (Figure 4). It can be seen that the temperature glide during evaporation is negligible compared to that during condensation. Therefore, as also published by other authors [3], a good glide matching during condensation, which results in a lower average heat rejection temperature of the cycle, is decisive for cycle efficiency. Figure 4b fairly shows the accordance in the slope of the temperature profile of heat sink and the most efficient mixture.

All in all, the results show that an increase in efficiency of nearly 1.3% (electricity) or 3% (CHP) is possible by using mixtures of MM and MDM, but, whether a use of mixtures is really advantageous or not depends, next to the pure thermodynamic performance, on several additional aspects. In this regard, the effect of an eventual composition shift on the cycle efficiency has to be considered. Moreover, the influence of mixtures on the performance of cycle components (e.g., the respective turbine efficiency) has to be evaluated. As heat transfer coefficients of mixtures are said to be lower than those of the pure components, it is crucial to investigate the required size of heat exchangers. In order to estimate this heat transfer area, proper correlations to describe the heat transfer characteristics are necessary. To identify them, measurements of heat transfer coefficients have to be conducted. The main parameter for a waste heat recovery system is the coupling with the heat source and, therefore, the evaporation process. Hence, this study focuses in a first step on evaporation heat transfer.

Figure 4. Temperature profiles during (a) evaporation and (b) condensation for the pure fluids as well as for the most efficient mixture (60 wt % MM) in case of CHP.

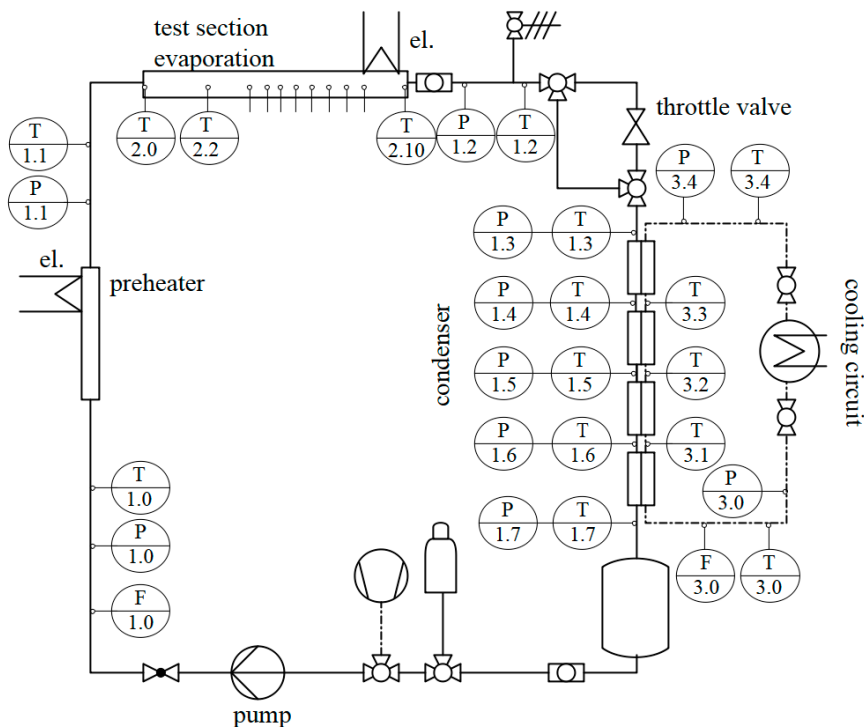


3. Heat Transfer Coefficients of Siloxanes and Siloxane Mixtures

3.1. Experimental Setup

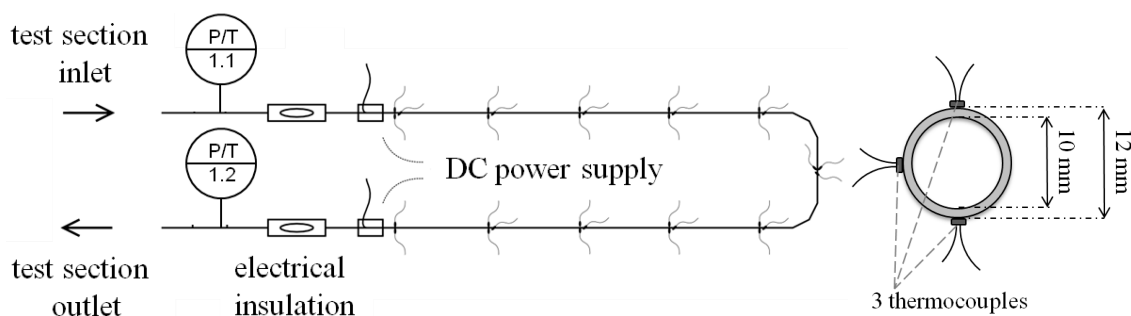
To measure the flow boiling heat transfer coefficients of the investigated siloxanes MM and MDM as well as their mixtures, a test rig (Figure 5) was built consisting of a pump, which raises the working fluid to the desired pressure, an electrically heated flow heater, which preheats the siloxane up to its saturation temperature, a test section, in which the fluid is evaporated, two expansion devices to reduce the pressure and a double-pipe heat exchanger to condense the fluid.

Figure 5. Test rig for measuring heat transfer coefficients.



All components and pipes are thermally isolated to the environment by a glass wool layer. The main test section (Figure 6) consists in a smooth, horizontal tube with one U-turn, which is electrically heated by Joule effect. It is electrically isolated from the rest of the test rig by a high-temperature plastic.

Figure 6. Test section for flow boiling.



Temperature and pressure is measured at the inlet as well as the outlet of the evaporator. Eleven measurement sites are placed alongside the evaporator in order to investigate heat transfer over the whole test section. At each measurement site three thermocouples are mounted at the tube. The overall outer wall temperature $T_{w,o}$ for one measurement site is therefore calculated by:

$$T_{w,o} = \frac{T_{w,t} + 2 \cdot T_{w,m} + T_{w,b}}{4} \quad (7)$$

using the temperatures at the top ($T_{w,t}$), middle ($T_{w,m}$) and bottom ($T_{w,b}$) of the tube.

The local heat transfer coefficient of evaporation h_{evap} is evaluated by:

$$h_{\text{evap}} = \frac{\dot{q}}{T_{w,i} - T_{\text{sat}}(x, p)} = \frac{\frac{P_{\text{el}}}{A}}{T_{w,i} - T_{\text{sat}}(x, p)} \quad (8)$$

Thereby, P_{el} corresponds to the power supplied by the DC power device. The temperature at the inner face of the tube, $T_{w,i}$, can be determined with respect to the outer wall temperature, $T_{w,o}$, by applying the law of heat conduction. T_{sat} represents the bulk temperature and therefore corresponds to the respective boiling point temperature, which depends on pressure and regarding mixtures as well on vapour quality. Its value is obtained by REFPROP (Reference Fluid Thermodynamic and Transport Properties Database) [27] assuming a linear pressure profile along the test section.

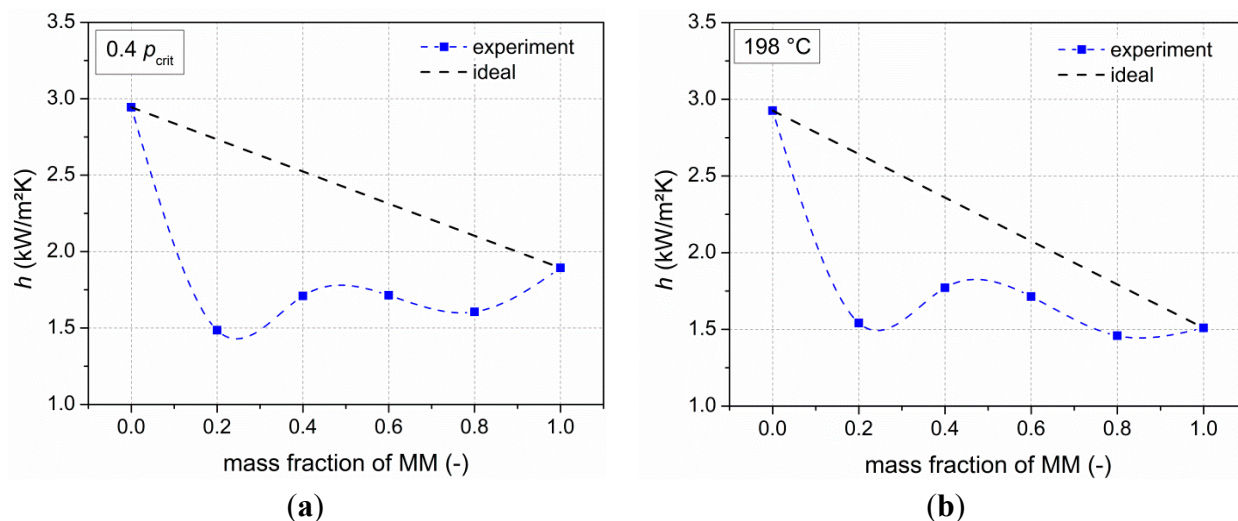
3.2. Experimental Results

Experiments have been performed at constant critical pressure as well as constant saturation temperature. Mixtures in steps of 20 wt % MM have been investigated. Figure 7 shows the results of the average heat transfer coefficients during evaporation with respect to mass fraction of MM. Respective uncertainties in measurements are below 30% [28].

It is obvious that the heat transfer coefficients of the siloxane mixtures deviate from the theoretical ideal values. The ideal curve is just a linear interpolation between the heat transfer coefficients of the pure components. In fact, it does not have any real physical meaning, but it can be used to describe the effect that the heat transfer coefficients of mixtures can be lower than those of the pure components. In case of constant reduced pressure, the maximum deviation of 46% occurs at 20% MM. The heat

transfer coefficient at constant saturation temperature deviates maximum 42% from the ideal value, again at 20% MM.

Figure 7. Average heat transfer coefficients for different mass fractions of MM at a pressure of (a) $0.4 p_{crit}$ [28] as well as (b) a saturation temperature of $198\text{ }^{\circ}\text{C}$.



3.3. Examination of Appropriate Correlations

A lot of different correlations for flow boiling of pure fluids as well as mixtures have been proposed during the last decades. Nevertheless, none of those correlations are based on high-temperature fluids like the investigated siloxanes. Due to that, as a basis, a correlation has to be chosen that offers a fluid-specific parameter in order to adjust it to the experimental data. Such correlations are given by Kandlikar [29] for pure fluids as well as mixtures. The investigation of the adaption of Kandlikar’s correlations to the experiments with siloxanes and their mixtures revealed that they are able to represent the general trend of heat transfer coefficient with respect to vapour quality and mass flux density quite well [28]. Therefore, the present study focuses on this correlation.

Regarding flow boiling in plain tubes, Kandlikar [29] suggests the following expression for the heat transfer coefficient of pure fluids (α_{TP}):

$$\alpha_{TP} = \max (\alpha_{NBD}, \alpha_{CBD}) \tag{9}$$

where α_{NBD} describes the heat transfer coefficient in the nucleate boiling region:

$$\alpha_{NBD} = 0.6683 Co^{-0.2}(1 - x)^{0.8} \alpha_{lo} + 1058.0 Bo^{0.7}(1 - x)^{0.8} F_{Fl} \alpha_{lo} \tag{10}$$

whereas α_{CBD} is used for regions where convective boiling is dominant:

$$\alpha_{CBD} = 1.136 Co^{-0.9}(1 - x)^{0.8} \alpha_{lo} + 667.2 Bo^{0.7}(1 - x)^{0.8} F_{Fl} \alpha_{lo} \tag{11}$$

In both cases the heat transfer coefficient with respect to vapour quality x depends on the convection number Co , the boiling number Bo as well as on a fluid-surface parameter F_{Fl} . For the single-phase heat transfer coefficient α_{lo} the correlations by Petukhov and Popov (Equation (12), for $0.5 \leq Pr_L \leq 2000$ and $10^4 \leq Re_{LO} \leq 5 \times 10^6$) or Gnielinski (Equation (13), for $0.5 \leq Pr_L \leq 2000$ and $2300 \leq Re_{LO} \leq 10^4$) are applied:

$$\alpha_{l_0,PaP} = \frac{\lambda_l}{d_i} \frac{Re_{l_0} Pr_L (f/2)}{1.07 + 12.7(Pr_L^{2/3} - 1)(f/2)^{0.5}} \quad (12)$$

$$\alpha_{l_0,G} = \frac{\lambda_l}{d_i} \frac{(Re_{l_0} - 1000) Pr_L (f/2)}{1.07 + 12.7(Pr_L^{2/3} - 1)(f/2)^{0.5}} \quad (13)$$

$$f = [1.58 \ln(Re_{l_0}) - 3.28]^{-2} \quad (14)$$

These correlations are based on the Reynolds number Re , the Prandtl number Pr and the friction factor f . In addition, the liquid thermal conductivity λ_l as well as the inner diameter d_i of the tube contribute to the heat transfer coefficient.

In case of fluid mixtures, Kandlikar distinguishes between three different regions according to the volatility parameter V_1 and the boiling number Bo [29]:

1. *Near azeotropic region*— $V_1 < 0.03$. In this domain the correlation for pure fluids is adopted (Equations (9)–(14)).
2. *Moderate diffusion-induced suppression region*— $0.03 < V_1 < 0.2$ and $Bo > 10^{-4}$. Heat transfer is dominated by convection. Therefore, Equation (12) is used to predict heat transfer coefficients.
3. *Severe diffusion-induced suppression region*— $0.03 < V_1 < 0.2$ and $Bo \leq 10^{-4}$ or $V_1 \geq 0.2$. This region is still dominated by convection. Moreover, additional mass diffusion resistance due to large composition differences has to be taken into account. Due to that, Equation (12) is extended by the diffusion-induced suppression factor F_D :

$$\alpha_{CBD} = 1.136 Co^{-0.9} (1 - x)^{0.8} \alpha_{l_0} + 667.2 Bo^{0.7} (1 - x)^{0.8} F_{Fl} \alpha_{l_0} F_D \quad (15)$$

$$F_D = \frac{0.678}{1 + V_1} \quad (16)$$

where the volatility parameter V_1 is defined by:

$$V_1 = \frac{c_{p,l}}{\Delta h_{LG}} \left(\frac{\kappa}{D_{12}} \right)^{0.5} \left| (y_1 - x_1) \left(\frac{dT}{dx_1} \right) \right| \quad (17)$$

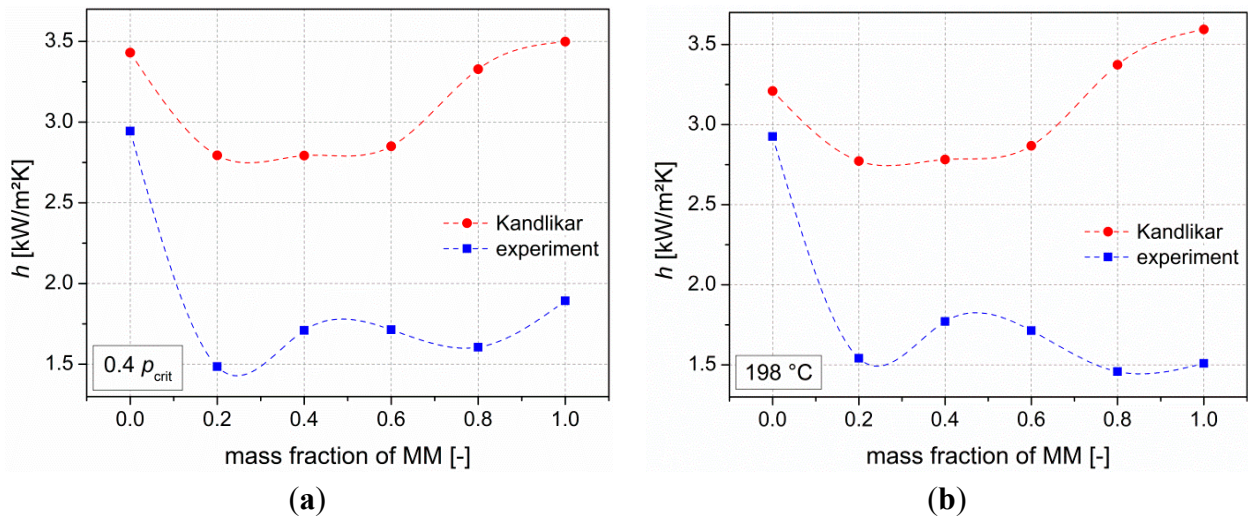
using the liquid specific heat $c_{p,l}$, the latent heat of vaporisation Δh_{LG} , the thermal diffusivity κ and the diffusion coefficient D_{12} . Moreover, the mass fraction of component 1 in vapour (y_1) and liquid (x_1) phase as well as the slope of the bubble point curve (dT/dx_1) contribute.

At first, Kandlikar's correlation was applied to the experimental test conditions while using $F_{Fl} = 1$ as suggested by Kandlikar for all fluids in stainless steel tubes. The results are demonstrated in Figure 8.

It can be seen that the absolute values between the correlation and the measurements differ, especially for the results of MM. For constant reduced pressure, the value of the experimental results of MM lies 46% below those of the correlation. In case of constant evaporation temperature the deviation is even 58%.

In order to obtain better agreement between the experimental and the theoretical heat transfer coefficients, the fluid-surface parameter F_{Fl} is used to adapt the values. It is fitted to the average heat transfer coefficients of the pure siloxanes.

Figure 8. Comparison of experimental results and Kandlikar’s correlation ($F_{Fl} = 1$): Average heat transfer coefficients for different mass fractions of MM at a pressure of (a) $0.4 p_{crit}$ as well as (b) a saturation temperature of $198\text{ }^{\circ}\text{C}$.



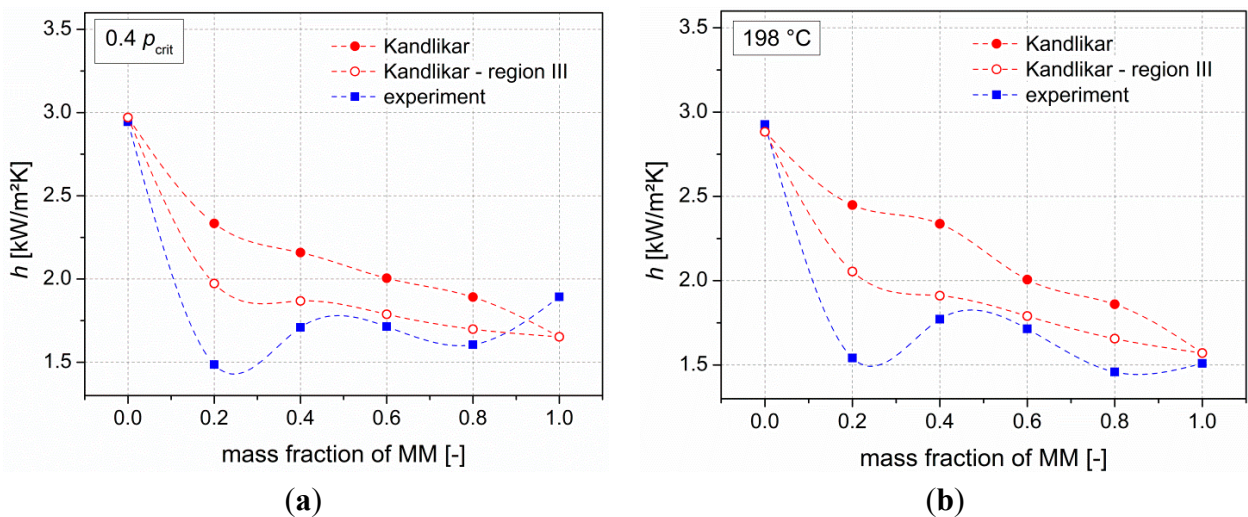
Using $F_{Fl,MM} = 0.1$ and $F_{Fl,MDM} = 0.8$ results in maximum deviations of 15% in case of MM and 1.5% regarding MDM. For mixtures, the fluid-surface parameter is derived from those of the pure components as suggested by Kandlikar:

$$F_{Fl, mixture} = x_{MM}F_{Fl,MM} + x_{MDM}F_{Fl,MDM} \tag{18}$$

Hereby, x_{MM} corresponds to the mass fraction of MM in liquid phase, x_{MDM} to that of MDM, respectively.

The results of applying these parameter values in the correlation are presented in Figure 9. The degradation in heat transfer coefficient in case of mixtures is small compared to the experimental data. In both cases, the mean deviations of the experimental data to the correlation are below 17%. Maximum deviations appear at 20% MM with a value of nearly -37% .

Figure 9. Comparison of experimental results and Kandlikar’s correlation ($F_{Fl,MM} = 0.1$, $F_{Fl,MDM} = 0.8$): Average heat transfer coefficients for different mass fractions of MM at a pressure of (a) $0.4 p_{crit}$ as well as (b) a saturation temperature of $198\text{ }^{\circ}\text{C}$.



Due to the investigated boundary conditions, only region I and II from Kandlikar's correlation are applied. As the experimental data still deviate from the adjusted correlation, the results by using the severe diffusion-induced suppression region (region III) (even though the volatility parameter or the Bo-Number would suggest another region) are analysed, too. The respective average heat transfer coefficients are added in Figure 9. By using this equation, maximum deviations of solely 25% are present. Mean deviations of the experimental data to the correlation are below 10%. Therefore, it is recommended to use the correlation given in region III together with the adjusted values of F_{Fl} when calculating heat transfer coefficients of MM/MDM-mixtures.

4. Estimation of Required Heat Exchanger Area

In order to reveal, whether the reduced heat transfer characteristics of fluid mixtures compensate their slight predominance in case of system efficiency, required heat exchange areas are investigated. For that purpose, a shell-and-tube heat exchanger with one shell pass and two tube passes is used as preheater and evaporator. Table 4 lists the main specifications and assumptions.

Table 4. Specifications and assumptions for the shell and tube heat exchanger.

Geometry Data			Maximum Velocities (m/s) [30,31]		
outer tube radius r_a (mm)	wall thickness Δd (mm)	thermal conductivity λ_{steel} (W/mK)	ORC liquid	ORC vapour	Dowtherm
9.5	2.1	15	4	20	4

The general approach for calculating the heat exchanger area is derived from Roetzel and Spang [32]. It is based on the Number of Transfer Units (NTU)-method. The NTU of the real shell and tube heat exchanger is obtained by applying a correction factor to the NTU of an ideal counterflow heat exchanger. For calculating the heat transfer coefficients at the inner and outer tube different models are applied. For Dowtherm G as well as for the ORC-fluid in the preheater, the correlation for turbulent flow by Gnielinski [33] is chosen, whereas for the evaporation of the ORC-fluid Kandlikar's correlation, as presented in Section 3, is used. The whole calculation is performed in Matlab [34]. Fluid properties are derived from REFPROP [27].

The calculations of required heat transfer area are performed for the pure fluids as well as for one more efficient mixture for the case of pure electricity and combined heat and power generation, respectively. Tables 5 and 6 list the respective process parameters that derived from the thermodynamic analysis in Section 2. These values represent the input parameters of the heat exchanger calculations.

Table 5. Process parameters for pure electric energy generation.

Fluid	\dot{m}_{TO} (kg/s)	T_{TO-IN} (K)	T_{TO-OUT} (K)	\dot{m}_{ORC} (kg/s)	$T_{ORC-R-E}$ (K)	$T_{ORC-E-T}$ (K)	p_{ORC} (bar)
MM	0.35	645.94	449.68	0.50	419.68	511.59	17.23
MDM	0.35	645.41	502.74	0.51	472.74	541.93	10.30
MM/MDM 95/05	0.35	646.32	452.51	0.50	422.51	513.32	16.92

Table 6. Process parameters for combined heat and power generation.

Fluid	\dot{m}_{TO} (kg/s)	T_{TO-IN} (K)	T_{TO-OUT} (K)	\dot{m}_{ORC} (kg/s)	$T_{ORC-R-E}$ (K)	$T_{ORC-E-T}$ (K)	p_{ORC} (bar)
MM	0.35	646.32	452.58	0.57	422.56	480.22	10.46
MDM	0.35	647.04	457.78	0.65	427.78	472.37	3.00
MM/MDM 60/40	0.35	645.99	450.09	0.57	420.30	480.90	6.77

The results of the heat exchanger analysis are summarised in Tables 7 and 8. In both cases MM requires the smallest heat transfer area. For pure electricity generation MDM shows the biggest heat exchanger areas. Regarding the evaporator (*EVAP*), 19% more heat compared to MM has to be transferred, but the heat transfer coefficient of evaporation exceeds that of MM by 53%. Due to that, an additional aspect has to contribute to the increased heat transfer area of 56%. Table 5 shows that mass flow rates of all three fluids are in the same range, but MDM shows the lowest pressure as well as temperature differences. Therefore, process parameters like temperatures and the respective fluid properties affect the required area just as well as pure heat transfer characteristics of fluids.

Table 7. Results of heat exchanger calculations for the case of pure electric power generation.

Pure Electricity	Heat Exchange Area (m ²)		Number of Tubes		Heat Transfer Coefficient (kW/m ² ·K) ORC/Dowtherm		Heat Duty (kW)	
	<i>PH</i>	<i>EVAP</i>	<i>PH</i>	<i>EVAP</i>	<i>PH</i>	<i>EVAP</i>	<i>PH</i>	<i>EVAP</i>
MM	0.725	0.120	2	2	5.761/7.202	26.414/8.343	113.35	30.725
MDM	0.741	0.187	2	2	5.141/7.450	40.502/8.256	86.901	36.500
MM/MDM 95/05	0.728	0.125	2	2	5.699/7.201	32.575/8.336	111.6	32.135

Table 8. Results of heat exchanger calculations for the case of combined heat and power generation.

CHP	Heat Exchange Area (m ²)		Number of Tubes		Heat Transfer Coefficient (kW/m ² ·K) ORC/Dowtherm		Heat Duty (kW)	
	<i>PH</i>	<i>EVAP</i>	<i>PH</i>	<i>EVAP</i>	<i>PH</i>	<i>EVAP</i>	<i>PH</i>	<i>EVAP</i>
MM	0.583	0.270	2	3	5.756/6.942	34.394/8.660	77.76	65.276
MDM	0.536	0.379	2	9	4.869/6.806	60.753/10.312	63.873	83.795
MM/MDM 60/40	0.602	0.373	2	4	5.245/6.762	37.859/8.914	64.009	80.192

In case of the mixture the evaporator needs a 4.2% enlarged area compared to that of MM. Process parameters are quite similar. The heat transfer coefficient of the mixture lies 23.3% above that of MM, whereas a higher heat duty of 4.6% is transferred. Together with slightly reduced temperature differences a higher area is required. Regarding the whole process of heat input using the mixture, 0.9% higher heat transfer areas result compared to MM.

For the case of the combined heat and power generation similar trends occur. Regarding the evaporator, MDM requires a 40.4% higher area than MM. Heat transfer coefficient is 76.6%, heat duty 28.4% above the values of MM. A 14% higher mass flow rate as well as again lower pressure and temperature differences affect the required area, too. As the number of tubes is set according to the maximum velocity in the tubes, more tubes are required in the evaporator for MDM due to higher mass flow rates. As the system pressure in case of combined heat and power generation is lower than in the

case of pure electricity generation, a higher part of the area is omitted to the evaporator due to increased heat of vaporisation.

The process parameters in case of the mixture again correspond more to those of MM. The heat duty in the evaporator exceeds that of MM by 22.9%. Heat transfer coefficients are 10.1% higher. An increase in heat transfer area of 38.15% is required. Again, compared to MM, slightly lower temperature differences and pressures are present. The total heat transfer area of preheater (*PH*) and evaporator exceeds that of MM by 14%.

Summing up it has to be stated that the pure heat transfer characteristics of fluids do not necessarily determine the size of the heat exchanger area. Process parameters play an even comparable role. For the investigated cases, the most efficient mixtures require an increase in heat transfer area for the heat input compared to the most efficient pure component of 0.9% and 14%, respectively. This corresponds to an increase in second law efficiency of 0.8% and 2.9%, respectively. As stated in the introduction, the potential of efficiency increase in high temperature ORC is low compared to low temperature applications. Heberle [35] reports an efficiency increase of almost 16% for a geothermal application using mixtures of R245fa and R365mfc. But the required heat transfer area (evaporator + preheater) for the most efficient mixture composition exceeds that of the most efficient pure fluid by 83% [35]. This effect is strongly influenced by the highly reduced heat transfer coefficients of R245fa/R365mfc-mixture compared to their pure components. Reductions compared to the pure fluids of up to nearly 50% are observed [36], whereas for the here investigated siloxane mixtures maximum deviations from the pure component with the lowest heat transfer coefficient are -21.5%. Therefore, it can be concluded, that even though comparably low efficiency increases are possible in high temperature applications, the required additional heat transfer area for mixtures is reduced compared to low temperature systems.

As the present investigations use an additional thermal oil loop, liquid heat transfer coefficients of heat source and ORC-fluid are quite similar. Therefore, the heat transfer coefficient of the ORC-fluid during evaporation can have a strong effect on the required heat transfer area. Regarding applications with direct use of exhaust gas, this effect is diminished or even negligible due to the generally low heat transfer characteristics of the exhaust gas. In these cases, already slight increases in efficiency by using mixtures can justify their application.

Next to the evaporation process, it is necessary to investigate the heat transfer areas of internal heat exchanger and condenser as well. As during internal heat exchange no phase change occurs, degradation of heat transfer coefficients of mixtures are not expected and, therefore, there should be no additional increase in heat transfer area. In contrary, during condensation, reduced heat transfer coefficients in case of mixtures are obvious. Thus, the heat transfer area of the condenser has to be calculated, too. In case of directly air cooled processes, the effect of heat transfer degradation of mixtures is again negligible due to the worse heat transfer characteristics of air. But, regarding the case of combined heat and power generation, where water is used as a cooling medium, the effect of the lower heat transfer coefficients of mixtures can again result in larger heat exchange areas.

5. Conclusions

The performance of the two linear siloxanes MM and MDM as well as their mixtures in a high temperature ORC are analysed using the example of waste heat from biogas plant. In case of pure electricity generation only slight improvements (1.3%) in second law efficiency can be achieved by using a mixture of 97 wt % MM. An efficiency increase of nearly 3% is obtained for the combined heat and power generation with the mixture 60/40-wt % MM/MDM. As the potential of efficiency increase drops with rising heat source temperature, these results seem reasonable compared to those given in literature.

Next to the thermodynamic analysis, measurements of heat transfer coefficients of the pure siloxanes as well as their mixtures (steps of 20 wt % MM) have been performed. Results show degradations of heat transfer coefficients compared to the ideal values of up to 46%. Kandlikar's correlation is used to describe the experimental data. In order to achieve a good agreement with the real values, the fluid-surface parameter was used to adjust the correlation. Moreover, the severe-diffusion induced region was chosen. By using this adapted correlation, mean deviations of less than 10% between the experimental data and the correlation are present.

Based on all these results, required heat transfer areas of evaporator and preheater are estimated assuming shell-and-tube heat exchangers. Calculations are performed for the case of pure electricity generation as well as combined heat and power generation for the pure components and one mixture. Results show an increased heat transfer area in case of the mixtures of around 1% (pure electricity, 95 wt % MM, efficiency increase: $\approx 1\%$) and 14% (combined heat and power, 60 wt % MM, efficiency increase: $\approx 3\%$). Moreover, it is obvious that next to the heat transfer coefficients, process parameters do have a strong influence on the required heat exchange area. Therefore, it cannot be stated that lower heat transfer coefficients lead to higher heat transfer areas than comparing a certain application. It is always necessary to calculate the respective areas under consideration of the (sometimes even just slightly) different operating conditions. However, it can be concluded that siloxanes, as working fluids for high temperature applications, exhibit reduced heat transfer degradation compared to low temperature fluids like for example R245fa/R365mfc. As a result, heat transfer areas are not as additionally increased as in case of geothermal applications and, therefore, the use of mixtures can be beneficial, even though efficiency increases are comparably small.

In order to definitely decide whether the use of mixtures is economically feasible in a certain application, it is certainly necessary to analyse the heat transfer areas of internal heat exchanger and condenser as well. In addition, the performance of turbine and pump has to be investigated, too. Finally, specific problems that can occur by using mixtures, as for example compositions shifts during the process, have to be analysed in detail. Therefore, in future work, analogous investigations (measurements of heat transfer coefficients, identifying of appropriate correlations as well as estimation of required heat transfer areas) will be performed with respect to the condenser. Then, a holistic evaluation of using mixtures in ORC-applications is possible.

Acknowledgments

The work was partially funded by the Deutsche Forschungsgemeinschaft (DFG) with project No. BR 1713/12. The authors gratefully acknowledge this support.

Author Contributions

All authors contributed to this work by collaboration. Theresa Weith is the main author of this manuscript. Florian Heberle assisted in the conceptual design of the study as well as in the experiments. Markus Preißinger particularly contributed to the heat exchanger model. The whole project was supervised by Dieter Brüggemann. All authors revised and approved the publication.

Conflicts of Interest

The authors declare no conflict of interest.

References

1. Heberle, F.; Preißinger, M.; Brüggemann, D. Zeotropic mixtures as working fluids in Organic Rankine Cycles for low-enthalpy geothermal resources. *Renew. Energy* **2012**, *37*, 364–370.
2. Aghahosseini, S.; Dincer, I. Comparative performance analysis of low-temperature Organic Rankine Cycle (ORC) using pure and zeotropic working fluids. *Appl. Therm. Eng.* **2013**, *54*, 35–42.
3. Liu, Q.; Duan, Y.; Yang, Z. Effect of condensation temperature glide on the performance of organic Rankine cycles with zeotropic mixture working fluids. *Appl. Energy* **2014**, *115*, 394–404.
4. Preißinger, M.; Heberle, F.; Brüggemann, D. Advanced Organic Rankine Cycle for geothermal application. *Int. J. Low Carbon Technol.* **2013**, *8*, i62–i68.
5. Chen, H.; Goswami, D.; Rahman, M.; Stefanakos, E. A supercritical Rankine cycle using zeotropic mixture working fluids for the conversion of low-grade heat into power. *Energy* **2011**, *36*, 549–555.
6. Baik, Y.-J.; Kim, M.; Chang, K.-C.; Lee, Y.-S.; Yoon, H.-K. Power enhancement potential of a mixture transcritical cycle for a low-temperature geothermal power generation. *Energy* **2012**, *47*, 70–76.
7. Yang, K.; Zhang, H.; Wang, Z.; Zhang, J.; Yang, F.; Wang, E.; Yao, B. Study of zeotropic mixtures of ORC (organic Rankine cycle) under engine various operating conditions. *Energy* **2013**, *58*, 494–510.
8. Zhang, J.; Zhang, H.; Yang, K.; Yang, F.; Wang, Z.; Zhao, G.; Liu, H.; Wang, E.; Yao, B. Performance analysis of regenerative organic Rankine cycle (RORC) using the pure working fluid and the zeotropic mixture over the whole operating range of a diesel engine. *Energy Convers. Manag.* **2014**, *84*, 282–294.
9. Angelino, G.; Colonna, P. Multicomponent Working Fluids for Organic Rankine Cycles (ORCs). *Energy* **1998**, *23*, 449–463.
10. Angelino, G.; Colonna, P. Air cooled siloxane bottoming cycle for molten carbonate fuel cells. In Proceedings of the Fuel Cell Seminar, Portland, OR, USA, 30 October 2000; pp. 667–670.

11. Dong, B.; Xu, G.; Cai, Y.; Li, H. Analysis of zeotropic mixtures used in high-temperature Organic Rankine cycle. *Energy Convers. Manag.* **2014**, *84*, 253–260.
12. Chys, M.; van den Broek, M.; Vanslambrouck, B.; de Paepe, M. Potential of zeotropic mixtures as working fluids in organic Rankine cycles. *Energy* **2012**, *44*, 623–632.
13. Kedzierski, M.; Kim, J.; Didion, D. Causes of the apparent heat transfer degradation for refrigerant mixtures. In Proceedings of the ASME/AIChe/ANS National Heat Transfer Conference, San Diego, CA, USA, 9–12 August 1992; pp. 149–158.
14. Stephan, K. Heat transfer in boiling of mixtures. In Proceedings of the Seventh International Heat Transfer Conference, Munich, Germany, 6–10 September 1982; pp. 59–81.
15. Bivens, D.; Yokozeki, A. Heat transfer of refrigerant mixtures. In Proceedings of the International Refrigeration and Air Conditioning Conference, Purdue University, West Lafayette, IN, USA, 14–17 July 1992; pp. 141–148.
16. Jung, D.; Song, K.; Ahn, K.; Kim, J. Nucleate boiling heat transfer coefficients of mixtures containing HFC32, HFC125, and HFC134a. *Int. J. Refrig.* **2003**, *26*, 764–771.
17. Li, M.; Dang, C.; Hihara, E. Flow boiling heat transfer of HFO1234yf and R32 refrigerant mixtures in a smooth horizontal tube: Part I. Experimental investigation. *Int. J. Heat Mass Transf.* **2012**, *55*, 3437–3446.
18. Choi, T.; Kim, Y.; Kim, M.; Ro, S. Evaporation heat transfer of R-32, R-134a, R-32/134a, and R-32/125/134a inside a horizontal smooth tube. *Int. J. Heat Mass Transf.* **2000**, *43*, 3651–3660.
19. Tibiriçá, C.; Ribatski, G. Flow boiling heat transfer of R134a and R245fa in a 2.3 mm tube. *Int. J. Heat Mass Transf.* **2010**, *53*, 2459–2468.
20. Ong, C.; Thome, J. Flow boiling heat transfer of R134a, R236fa and R245fa in a horizontal 1.030 mm circular channel. *Exp. Therm. Fluid Sci.* **2009**, *33*, 651–663.
21. Fernández, F.; Prieto, M.; Suárez, I. Thermodynamic analysis of high-temperature regenerative organic Rankine cycles using siloxanes as working fluids. *Energy* **2011**, *36*, 5239–5249.
22. Lai, N.; Wendland, M.; Fischer, J. Working fluids for high-temperature organic Rankine cycles. *Energy* **2011**, *36*, 199–211.
23. Heberle, F.; Preißinger, M.; Weith, T.; Brüggemann, D. Experimental Investigation of Heat Transfer Characteristics and Thermal Stability of Siloxanes. Available online: <http://www.asme-orc2013.nl/uploads/File/PPT%20082.pdf> (accessed on 21 June 2014).
24. The Dow Chemical Company. Dowtherm G, Product Information. Available online: http://msdssearch.dow.com/PublishedLiteratureDOWCOM/dh_0033/0901b803800337f0.pdf?filepath=heattrans/pdfs/noreg/176-01466.pdf&fromPage=GetDoc (accessed on 19 May 2014).
25. Aspen Technology, Incorporation. *Aspen One V 7, Process Optimization for Engineering, Manufacturing, and Supply Chain, Aspen Plus V 7.3*; Aspen Technology: Burlington, ON, Canada, 2011.
26. Aspen Technology, Incorporation. *Aspen Physical Property System. Physical Property Methods. Documentation to Aspen Plus V 7.3*; Aspen Technology: Burlington, ON, Canada, 2011.
27. Lemmon, E.W.; Huber, M.L.; McLinden, M.O. *NIST Standard Reference Database 23: Reference Fluid Thermodynamic and Transport Properties-REFPROP, Version 9.1*; National Institute of Standards and Technology, Standard Reference Data Program: Gaithersburg, MD, USA, 2013.

28. Weith, T.; Heberle, F.; Brüggemann, D. Experimental Investigation of Flow Boiling Characteristics of Siloxanes and Siloxane Mixtures in a Horizontal Tube. In Proceedings of the International Symposium on Convective Heat and Mass Transfer, CONV-14, Kusadasi, Turkey, 8–13 June 2014.
29. Kandlikar, S. Boiling heat transfer with binary mixtures: Part II—Flow boiling in plain tubes. *J. Heat Transf.* **1998**, *120*, 388–394.
30. Podhorsky, M.; Krips, H. *Wärmetauscher—Aktuelle Probleme der Konstruktion und Berechnung*, 2nd ed.; Vulkan-Verlag: Essen, Germany, 1999. (In German)
31. Wolf, P.; Kirchner, G.O. Konstruktive Hinweise für den Bau von Wärmeübertragern. In *VDI-Wärmeatlas*, 10th ed.; Verein Deutscher Ingenieure: Berlin, Germany, 2013. (In German)
32. Roetzel, W.; Spang, B.C. Berechnung von Wärmeübertragern. In *VDI-Wärmeatlas*, 10th ed.; Verein Deutscher Ingenieure: Berlin, Germany, 2013. (In German)
33. Gnielinski, V. Ein neues Berechnungsverfahren für die Wärmeübertragung im Übergangsbereich zwischen laminarer und turbulenter Rohrströmung. *Forsch. Geb. Ing.* **1995**, *61*, 240–248. (In German)
34. MathWorks, Inc. *MATLAB R2010b*; MathWorks, Inc.: Natick, MA, USA, 2010.
35. Heberle, F. Untersuchungen zum Einsatz von zeotropen Fluidgemischen im Organic Rankine Cycle für die geothermische Stromerzeugung. Ph.D. Thesis, Universität Bayreuth, Bayreuth, Germany, 2013. (In German)
36. Heberle, F.; Brüggemann, D. Pool boiling heat transfer coefficients of R245fa, R365mfc and their mixtures. In Proceeding of the 8th World Conference on Experimental Heat Transfer, Fluid Mechanics, and Thermodynamics, Lisbon, Portugal, 16–20 June 2013.

© 2014 by the authors; licensee MDPI, Basel, Switzerland. This article is an open access article distributed under the terms and conditions of the Creative Commons Attribution license (<http://creativecommons.org/licenses/by/3.0/>).